Colloid Polym Sci (2006) 285: 11–17
DOI 10.1007/s00396-006-1475-x

ORIGINAL CONTRIBUTION

Wei-Min Hou
Gang Liu
Jian-Jun Zhou
Xia Gao
Yan Li
Lin Li
Shi Zheng
Zhong Xin
Li-Qun Zhao

The influence of crystal structures of nucleating agents on the crystallization behaviors of isotactic polypropylene

Received: 6 December 2005
Accepted: 11 February 2006
Published online: 17 August 2006

W.-M. Hou · G. Liu · J.-J. Zhou (✉) · X. Gao · Y. Li · L. Li
State Key Laboratory of Polymer Physics and Chemistry, Institute of Chemistry, Chinese Academy of Sciences,
Beijing 100080, China
e-mail: pla_zjj@iccas.ac.cn

S. Zheng · Z. Xin
College of Chemical Engineering, East China University of Science and Technology,
Shanghai 200237, China

L.-Q. Zhao
College of Chemical Engineering,
Shenyang Institute of Chemical Technology,
Liaoning 110021, China

W.-M. Hou · G. Liu
Graduate School, Chinese Academy of Sciences,
Beijing 100080, China

Abstract The crystals of N, N′-dicyclohexyl-2,6-naphthalenedicarboxamide (DC26NDCA) and N,N′-dicyclohexyl-1,4-naphthalenedicarboxamide (DC14NDCA) were selected as nucleating agents to induce the crystallization of isotactic polypropylene (*i*-PP). The influence of the crystal structures of the nucleating agents on the crystallization behaviors and morphologies was studied by means of differential scanning calorimeter, wide-angle X-ray diffraction, polarized light microscopy, and atomic force microscopy (AFM). The results show that DC26NDCA is a selective β-nucleating agent for the *i*-PP crystallization, while DC14NDCA only has a very weak α-nucleating effect for the *i*-PP crystallization. The dynamic growth processes reveal that *i*-PP crystals grow with different crystallization behaviors in the presence of the nucleating agents. The *i*-PP lamellar structures on the crystal surfaces of the nucleating agents were observed by AFM in details, which suggested that the nucleating agents induced the epitaxial growth of the *i*-PP lamellae.

Keywords Isotactic polypropylene · Nucleating agent · Epitaxial growth · Crystallization

Introduction

Isotactic polypropylene (*i*-PP) is a semicrystalline polymer with several crystal modifications such as α, β, and γ. The formation of various crystal modifications is depended on the crystallization conditions [1–4]. When crystallized from the melt, the α-form can easily be obtained. The β-form can be formed by various methods such as temperature gradient [5] crystallized from oriented melt [6] or adding a selective β-nucleating agent [7–14]. An effective nucleating agent can significantly reduce the induction time of crystallization because it can provide extra-surfaces onto which the epitaxial growth of *i*-PP lamellae can be initiated [14–17]. Therefore, a specific crystal modification of *i*-PP can be formed by controlling the crystallization conditions and using a selective nucleating agent. Many studies were conducted on the effect of the nucleating agents for *i*-PP crystallization such as the influence of the nucleating agents on crystallization rate and the formation of a specific crystal modification. The mechanism of the nucleating agents inducing the epitaxial growth was studied in the recent years [14, 16, 18–36]. By comparing the effects of various nucleating agents, Garbarczyk and Paukszta [18] suggested that the molecular structure and crystal shape of nucleating agents can be related to the space arrangements of *i*-PP chains during crystallization. Kawai et al. [16] studied the alignment of the *i*-PP crystals induced by N, N′-dicyclohexyl-2,6-naphthalenedicarboxa-

mide (DC26NDCA) under a magnetic field. Their results revealed that on the epitaxial surfaces, the *c*-axis of the β-form *i*-PP modifications aligns parallel to the *b*-axis of the nucleating agent and the molecular packing of the β-form *i*-PP exhibits a good matching with the surface of the DC26NDCA. Stocker et al. [14] observed the epitaxial growth of β-form *i*-PP on the crystal of a nucleating agent by transmission electron microscope (TEM). Their results show that the nucleating agent with about 6.5 Å periodicity and orthogonal geometry of the contact face is likely to induce the β-form *i*-PP crystals. However, the details of the crystal of the nucleating agent might be damaged during sample preparation for the TEM observations. A direct observation on the epitaxial growth of lamellae of *i*-PP crystals initially induced on the surface of a nucleating agent is of great importance.

In this paper, the influences of two nucleating agents DC26NDCA and N,N′-dicyclohexyl-1,4-naphthalenedicarboxamide (DC14NDCA) on the crystallization of *i*-PP are studied. The epitaxial growth of *i*-PP lamellae on the surfaces of the nucleating agents is observed directly by atomic force microscopy (AFM).

Experimental section

i-PP was supplied by Yanshan Petrochemical Co., with M_n=76,000, M_w/M_n=5.4, and T_m=163 °C. Nucleating agents DC26NDCA and DC14NDCA were synthesized in our laboratory. The molecular structures are shown in Scheme 1. The *i*-PP pellets with 0.1 wt% nucleating agent were mixed at 210 °C using a ThermoHaake Rheomix 600P twin-screw mixer. Thin films for the AFM observation were prepared by spin coating polymer solutions onto a freshly cleaved surface of mica on which the powder of the nucleating agents was added. The *i*-PP was dissolved in boiling *p*-xylene (138 °C) with a concentration of 10 mg ml^{-1}. To obtain a smooth surface of *i*-PP thin films, the mica substrate was heated to 80 °C during the spin coating to evaporate *p*-xylene quickly. The samples were directly crystallized from the melt in the differential scanning calorimeter (DSC) cell via melting at 200 °C for 5 min and cooling to the crystallization temperature of 130 °C at which the samples were held for a specified time.

The thermal behavior was investigated using a DSC (TA DSC2910) under nitrogen purge (50 ml min^{-1}). Temperature calibration was performed with an indium standard before use. The melting temperatures (T_m) and crystallization temperatures (T_c) were obtained with DSC scanning rate at 10 °C min^{-1}. For isothermal crystallization, the samples were melted in the DSC cell at 200 °C for 5 min and then quickly cooled to a selected temperature for crystallization. Wide-angle X-ray diffraction (WAXD) was performed on Rigaku D/max-2500 X-ray diffractometer using Ni-filtered Cu Kα radiation (λ=0.1542 nm) operated at 40 kV and 60 mA. The scanning range is from 0 to 60° and the scanning step is 0.02°. The crystallization processes of the *i*-PP samples with and without the nucleating agents were observed by polarized optical microscopy (POM) (Olympus BH-2, Japan) equipped with a Panasonic 230 CCD camera. AFM observations were performed with Nanoscope III MultiMode scanning probe microscope (Digital Instruments, Santa Barbara, CA, USA) equipped with a vertical J scanner. The results were obtained in tapping mode AFM using silicon tips (TESP, Digital Instruments) with a resonance frequency of approximately 300 kHz and a spring constant of about 40 N m^{-1} were used. Height and phase images were taken simultaneously. All images were taken with 512 lines by 512 lines. The images shown here were subjected to a first-order plane fitting and first-order flattening procedures to compensate for the sample tilt.

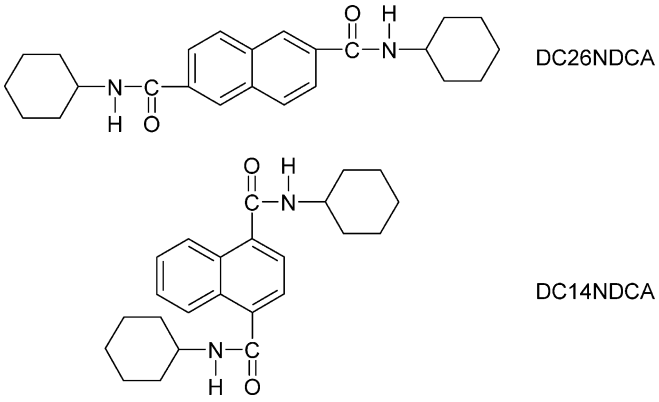

Scheme 1 The chemical structures of the nucleating agents

Results and discussion

Thermal analysis Figure 1a shows the thermal behaviors of *i*-PP, *i*-PP/DC14NDCA, and *i*-PP/DC26NDCA, which were obtained by directly crystallizing from the melt via melting at 200 °C for 5 min and cooling at 10 °C min^{-1}. The maximums of the exothermic peaks (T_c) corresponding to the largest crystallization rate are 110.2, 116.2, and 126.6 °C of the *i*-PP, *i*-PP/DC14NDCA, and *i*-PP/DC26NDCA, respectively. It can be seen that the T_c of the *i*-PP/DC26NDCA is significantly higher than that of pure *i*-PP. For the samples of *i*-PP/DC14NDCA, a slight increase in the T_c is observed compared with that of the pure *i*-PP. It is known that the higher the T_c, the lower the nucleation barrier. Therefore, it suggested that both the DC14NDCA and DC26NDCA can induce the nucleation of *i*-PP and enhance the crystallization rate of *i*-PP. The nucleation efficiency of DC26NDCA is higher than that of DC14NDCA. At the end of the nonisothermal crystallization, the melting endotherms of *i*-PP, *i*-PP/DC14NDCA, and *i*-PP/DC26NDCA were obtained by immediate heating at a rate of 10 °C min^{-1} as shown in Fig. 1b. It can be seen

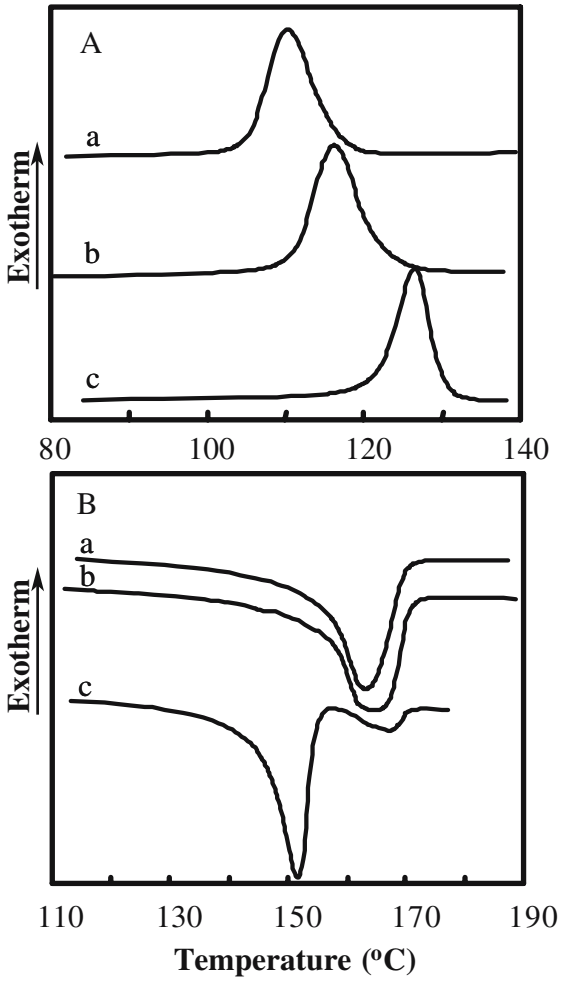

Fig. 1 **a** Plots of crystallization temperature and **b** melting temperature of curves **a***i*-PP, **b***i*-PP/DC14NDCA, and **c***i*-PP/DC26NDCA

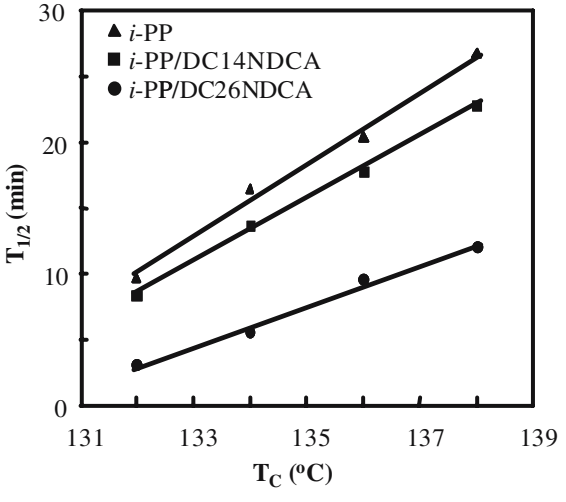

Fig. 2 Half time of crystallization ($t_{1/2}$) vs crystallization temperature (T_c) for *i*-PP, *i*-PP/DC14NDCA, and *i*-PP/DC26NDCA

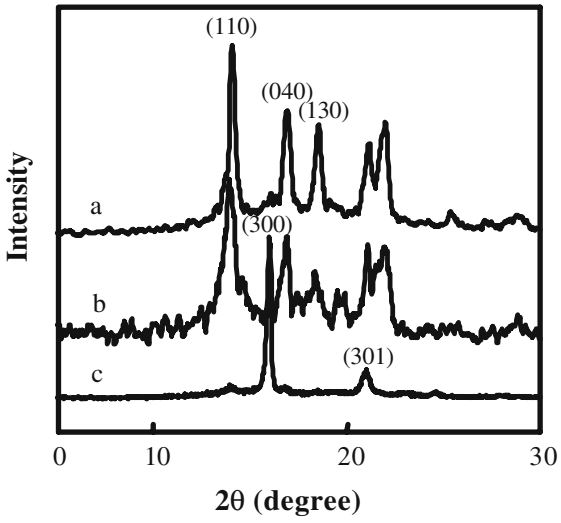

Fig. 3 Wide-angle X-ray diffraction patterns: **a***i*-PP, **b***i*-PP/DC14NDCA, and **c***i*-PP/DC26NDCA

that only the *i*-PP/DC26NDCA sample exhibits double melting endotherms at 151.5 and 167.2 °C, which correspond to the melting points of the β- and the α-form *i*-PP crystals, respectively. A single melting peak of the pure *i*-PP and *i*-PP/DC14NDCA that is related to the melting point of the α-form *i*-PP crystal was observed at 163.2 and 164.1 °C, respectively. It indicates that the β-form *i*-PP crystals can mainly be obtained for the *i*-PP/DC26NDCA and only the α-form *i*-PP crystals can be formed for the *i*-PP/DC14NDCA when the samples are crystallized under the same condition.

Isothermal crystallization of the *i*-PP, *i*-PP/DC14NDCA, and *i*-PP/DC26NDCA samples was investigated in the temperature range from 132 to 138 °C. The relation between the half time ($t_{1/2}$) and T_c is shown in Fig. 2. It can be found that the $t_{1/2}$ decreases greatly for the samples of *i*-PP/DC26NDCA and *i*-PP/DC14NDCA compared with the pure *i*-PP at the same crystallization temperature. It reveals that the addition of the nucleation agents can significantly enhance the nucleation density to increase the overall crystallization rate of *i*-PP and the crystallization rate enhanced by the DC26NDCA is much higher than that by the DC14NDCA.

Crystal structure and morphology Figure 3 shows the WAXD patterns of the *i*-PP, *i*-PP/DC14NDCA, and *i*-PP/DC26NDCA samples. The WAXD patterns of pure *i*-PP and *i*-PP with DC14NDCA show identical reflection peaks at 2θ=14.1, 17.0, and 18.6°. Those peaks correspond to the (110), (040), and (130) planes of the α-form modifications of *i*-PP crystals, respectively. From the diffraction pattern of the *i*-PP with DC26NDCA, two main reflections are clearly observed at 2θ=16.0 and 21.1° as shown in Fig. 3c. According to the characteristic reflection peaks of *i*-PP crystals, the two reflection peaks are

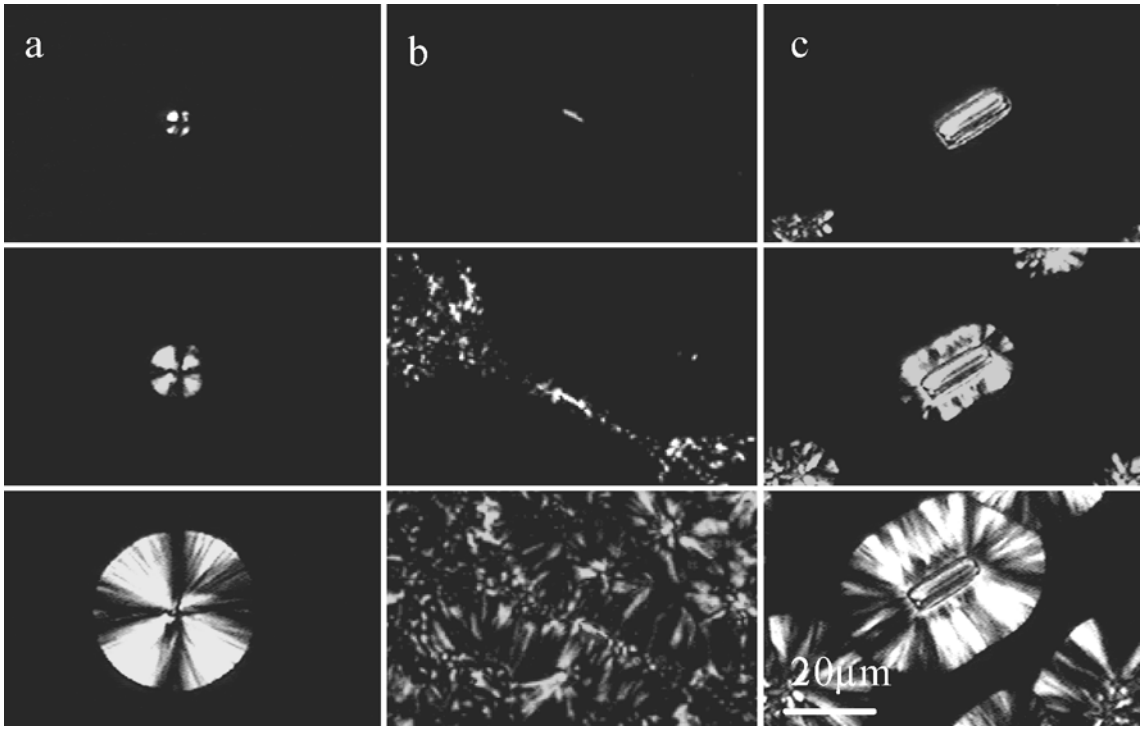

Fig. 4 The dynamic growth processes of spherulites under polarized light: **a***i*-PP, **b***i*-PP/DC14NDCA, and **c***i*-PP/DC26NDCA

associated with the (300) and (301) planes of the β-form *i*-PP crystals. It indicates that the β-form crystals of *i*-PP can be easily developed by adding the nucleating agent of DC26NDCA and the DC14NDCA cannot induce the formation of the β-form crystals, which only show a weak effect on the nucleation of α-form crystals of *i*-PP.

The dynamic growth processes of spherulites of the *i*-PP, *i*-PP/DC14NDCA, and *i*-PP/DC26NDCA films were observed by a POM with a hot stage as shown in Fig. 4. Figure 4a shows the spherulitic growth process of a pure *i*-PP film that was crystallized at 130 °C. The α-form spherulite with clear Maltese cross was obtained and the negative birefringence was observed when a color-sensitive plate was inserted. The growth process of the spherulites of *i*-PP induced by DC14NDCA was shown in Fig. 4b. In the center of Fig. 4b, a rectangular crystal of the DC14NDCA can be seen. When crystallized at 130 °C, it is found that two leading groups of lamellar sheaves spread out from the ends of the DC14NDCA crystal. The lamellar sheaves branched, bent, and developed into mature spherulites. Usually, the DC14NDCA crystals can induce the formation of the mixed-type α-form spherulites with random blue and yellow colors in the same quadrant when the color-sensitive plate was inserted. It can be assumed that the DC14NDCA crystal can provide foreign surfaces onto which the *i*-PP chains can deposit. Figure 4c shows the growth process of an *i*-PP spherulite induced by the DC26NDCA. When crystallized at 130 °C, it is found that the *i*-PP spherulite initially grows out from some sides of a rectangular DC26NDCA crystal surface. The spherulite develops until it grows on the fronts and impinges on other ones. It is clearly seen that nucleation of the DC14NDCA in the *i*-PP crystallization process shows a significant difference from that of the DC26NDCA. The DC26NDCA crystals can provide numerous nucleation points to induce the epitaxial growth of the β-form *i*-PP crystals and the DC14NDCA crystals can only provide limited nucleation points to promote the formation of the α-form *i*-PP crystals, which agrees well with our previous DSC results.

Lamellar structures Figure 5 shows the lamellar structures of the α- and β-form spherulites of pure *i*-PP samples. It was found that the cross-hatched lamellae in the mixed-type α-form spherulites can be observed by AFM phase imaging as indicated by an arrow in Fig. 5b. Moreover, in some sectors of the mixed-type α-form spherulites, the lath-like lamellae can be found as indicated by arrows in Fig. 5c. The lamellar structures of the β-form spherulites are dominant by the parallel edge-on lamellae with occasional lamellar branches in some sectors, while in the other sectors, the flat-on lamellae with giant screw dislocations can be found as shown in Fig. 5d–f. Our results clearly show that the lamellar structures of the α- and β-form *i*-PP spherulites can be easily discriminated by AFM phase imaging.

To further investigate the induced lamellar growth of the α- and β-forms of *i*-PP crystals on the faces of the

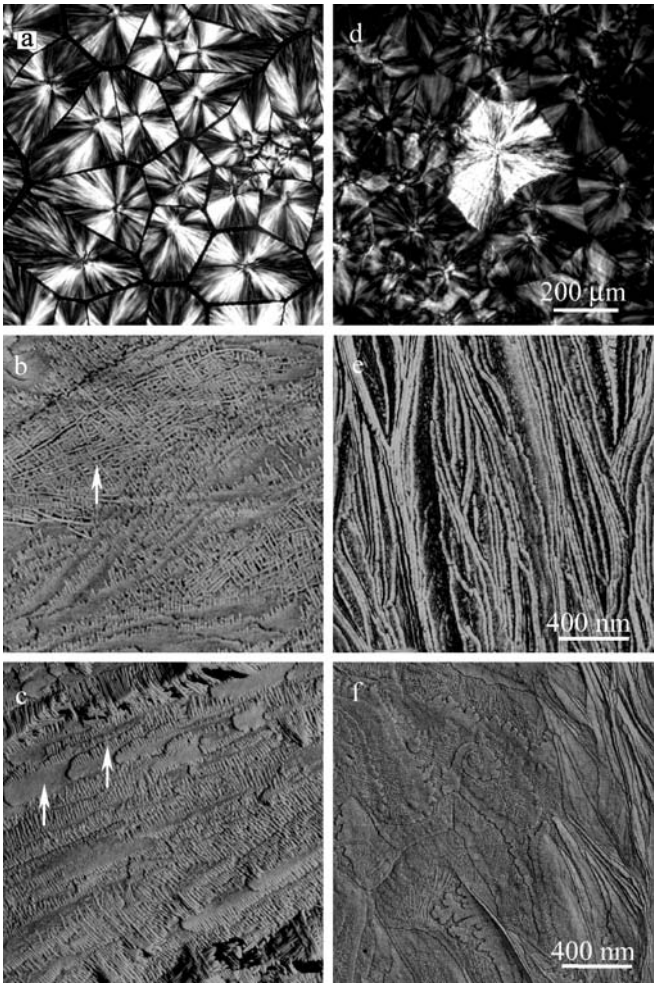

Fig. 5 The lamellar structures of the α and β-form spherulites of pure *i*-PP samples

DC14NDCA and DC26NDCA crystals, the contact surfaces of the DC14NDCA and DC26NDCA crystals on which the *i*-PP films crystallized were observed by AFM phase imaging. An interface of the *i*-PP lamellae (labeled by "PP") and the DC14NDCA crystals (labeled by "NA") was directly observed by AFM as shown in Fig. 6. It can be seen that there is a gap between the *i*-PP lamellae and one of the surfaces of the DC14NDCA crystal. It is suggested that the *i*-PP lamellae cannot be induced by most exposed planes of the DC14NDCA crystal, although some connected structure can be occasionally seen on that plane of the DC14NDCA crystal as indicated by arrows in Fig. 6a. On the other plane of the DC14NDCA crystal, the *i*-PP lamellae were induced and developed to form the lath-like lamellae as indicated by arrows in Fig. 6c,d. It seems that the DC14NDCA crystal only provided few foreign surfaces to induce the growth of *i*-PP lamellae. The chains of *i*-PP might be easier to deposit onto certain crystal planes of the DC14NDCA crystal to develop some heterogeneous nuclei and then the

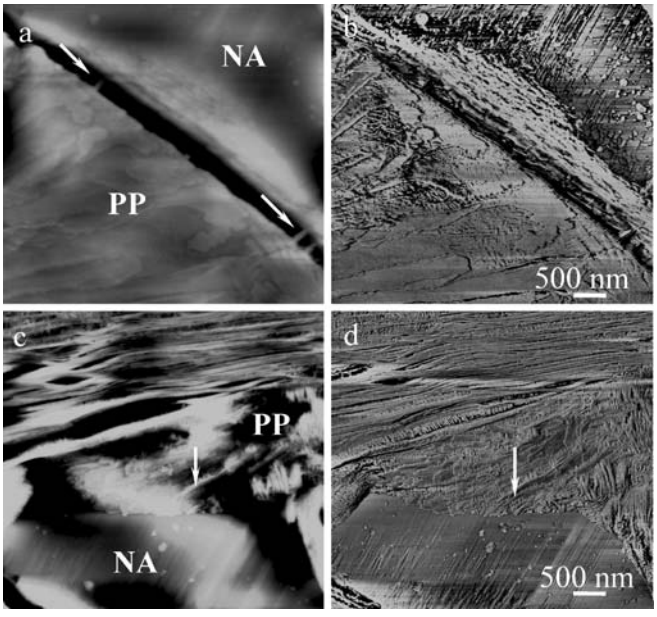

Fig. 6 AFM height and phase images of the interface of the *i*-PP lamellae and the DC14NDCA crystal

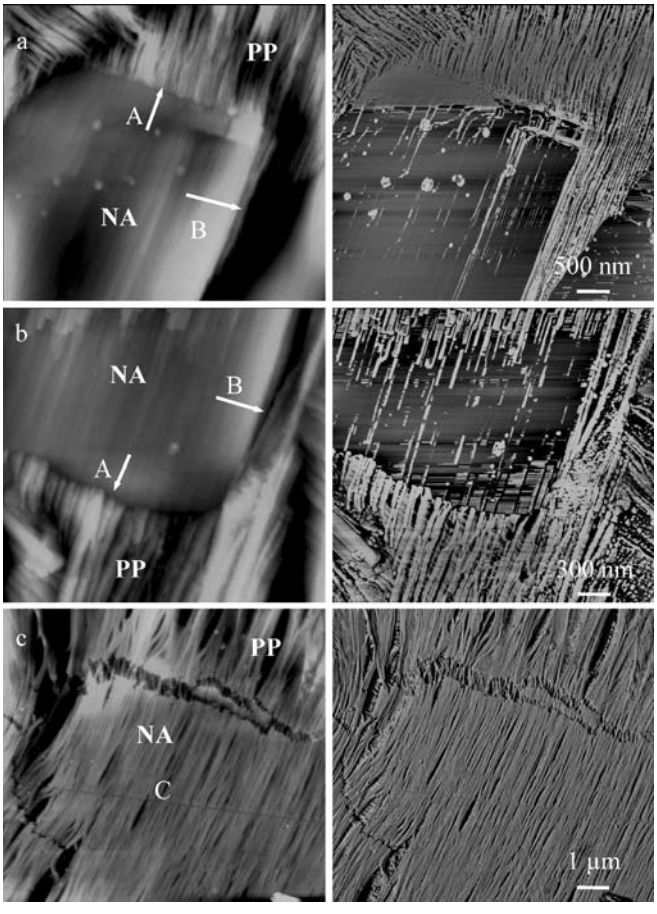

Fig. 7 AFM height and phase images of the interface of the *i*-PP lamellae and the DC26NDCA crystal

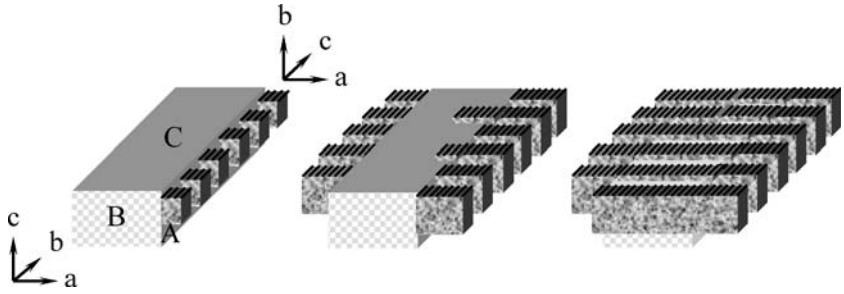

Fig. 8 Schematic illustration of the epitaxial lamellar growth of the β-form crystals of *i*-PP induced by the DC26NDCA crystal

i-PP lamellae can develop. Therefore, only the α-form crystals of *i*-PP were observed in the *i*-PP films with the DC14NDCA crystals.

Figure 7 is an interface of the *i*-PP lamellae and a DC26NDCA crystal observed by AFM. It can be observed that the *i*-PP lamellae can epitaxially crystallize on the lateral planes of the DC26NDCA crystal. The edge-on lamellae of *i*-PP were clearly seen growing directly on one of the lateral surfaces of the DC26NDCA crystal as indicated by arrow A in Fig. 7a,b. Moreover, the edge-on lamellae are parallel each other and perpendicular to the "A" plane of the contact faces. While on the other lateral plane (marked by arrow B), the edge-on lamellae are parallel the "B" lateral plane and their original orientation direction does not change. Our observations suggest that the B lateral plane of the DC26NDCA crystal cannot induce the epitaxial growth and the orientation alignment of the *i*-PP lamellae. To study the lamellar growth on the "C" lateral plane of the DC26NDCA crystal (marked by C in Fig. 7c), a thin layer of the *i*-PP film was covered on top of the DC26NDCA crystal. The orientation of *i*-PP lamellae on top of the C lateral plane of the DC26NDCA crystal is shown in Fig. 7c. The edge-on lamellae of *i*-PP are all parallel to each other and the orientation alignment of the *i*-PP lamellae on top of the C lateral plane of the DC26NDCA crystal is similar to that on the B lateral plane as clearly shown in the AFM phase image of Fig. 7c. Therefore, our AFM observations reveal that only the A lateral plane of the DC26NDCA crystal can induce the epitaxial growth of *i*-PP lamellae. The edge-on lamellae of *i*-PP induced by the DC26NDCA crystals without the crosshatched and lath-like lamellae suggested that only the β-form crystals of *i*-PP were formed as shown in the AFM phase images of Figs. 5 and 7.

It was reported that the DC26NDCA crystals can induce the epitaxial crystallization of the β-form crystals of *i*-PP. Recently, Kawai et al. [16] discussed the epitaxial growth of the β-form crystals of *i*-PP on the surface of the DC26NDCA crystal in details. They proposed that the *c*-axis of the *i*-PP lies parallel to the *b*-axis of the DC26NDCA crystal; the methyl groups of *i*-PP helix are fitted to the periodic cavities on the *bc*-plane of the DC26NDCA. The length of the *c*-axis corresponding to the period of the 3_1 helix of *i*-PP is 6.49 Å, while the length of the *b*-axis of the DC26NDCA is 6.687 Å. These two values are fairly close so the epitaxial crystallization between the β-form crystals of *i*-PP and the DC26NDCA can take place. While the misfit factor between the α-form crystals of *i*-PP and the DC26NDCA is too big to fit each other, the epitaxial crystallization between the α-form crystals of *i*-PP and the DC26NDCA cannot occur. According to our AFM observations and the arguments by Kawai et al., the A lateral plane is the *bc*-plane of the DC26NDCA crystal. The epitaxial nucleation of the β-form crystals of *i*-PP initially formed on the A lateral plane (*bc*-plane) of the DC26NDCA crystal is the parallelism of the *b* and *c* axes of the nuclei of the β-form crystals with the *c* and *b* axes of the DC26NDCA crystal, respectively, of the other. The nuclei further grew and developed to form lamellar sheaves that are perpendicular to the A lateral plane and parallel to the B and C lateral planes of the DC26NDCA crystal as illustrated in Fig. 8. The crystal structure of the DC14NDCA was characterized by single crystal X-ray diffraction methods. The parameters of the crystal structures of the *i*-PP, DC14NDCA, and DC26NDCA crystals are summarized in Table 1. It can be seen that the unit cell parameters misfit between the DC14NDCA and the α- or β-form crystals of *i*-PP. Therefore, it is reasonable to find that the DC14NDCA crystal can induce quite a few nuclei of the α-form and no nuclei of the β-form crystals of *i*-PP. Our experiments suggest that the crystal structure of a nucleating agent plays a dominant role on the crystallization behaviors of *i*-PP.

Table 1 The parameters of crystal structures of *i*-PP, DC14NDCA, and DC26NDCA

Parameter	α-form of *i*-PP	β-form of *i*-PP	DC14NDCA	DC26NDCA
	Monoclinic	Trigonal	Triclinic	Monoclinic
a	6.65	11.01	10.29	5.12
b	20.96	11.01	10.92	6.69
c	6.50	6.50	18.15	29.07
α			98.70	
β	99.2		96.55	91.09
γ			90.14	

Conclusion

Our results indicate that the DC26NDCA and DC14NDCA crystals have considerably different influences on the crystallization behaviors of *i*-PP even though they have similar molecular structures. The DC26NDCA crystals can induce the formation of β-form crystals of *i*-PP, while the DC14NDCA crystals show only limited nucleation effect on the formation of α-form crystals of *i*-PP. AFM investigations reveal that the epitaxial nucleation of the β-form crystals of *i*-PP initially formed on a specific lateral plane of the DC26NDCA crystal. It can be concluded that the formation of a specific form crystal of *i*-PP is mainly related with the crystal structures of nucleating agents.

Acknowledgements We are grateful for the support of the Outstanding Youth Found and National Science Foundation of China (Grant nos. 20574083, 20325414, and 50521302).

References

1. Turner Jones A, Aizlewood JM, Beckett DR (1964) Makromol Chem 75:134
2. Norton DR, Keller A (1985) Polymer 26:704
3. Thomann R, Wang C, Kressler J, Mülhaupt R (1996) Macromolecules 29:8425
4. Ullmann W, Wendorff JH (1979) Prog Colloid & Polym Sci 66:25
5. Lovinger AJ, Chua JO, Gryte CC (1977) J Polym Sci Part B Polym Phys 15:641
6. Leugering HJ, Kirsch G (1973) Angew Makromol Chem 33:17
7. Varga J (2002) J Macromol Sci Part B Phys 41:1121
8. Varga J, Tóth FS (1991) Angew Makromol Chem 188:11
9. Varga J, Mudra I, Ehrenstein GW (1999) J Appl Polym Sci 74:2357
10. Marco C, Gómez MA, Ellis G, Arribas JM (2002) J Appl Polym Sci 86:531
11. Huang MR, Li XG, Fang BR (1995) J Appl Polym Sci 56:1323
12. Garbarczyk J, Paukszta D (1985) Colloid Polym Sci 263:985
13. Mathieu C, Thierry A, Wittmann JC, Lotz B (2002) J Polym Sci Part B Polym Phys 40:2504
14. Stocker W, Schumacher M, Graff S, Thierry A, Wittmann JC, Lotz B (1998) Macromolecules 31:807
15. Zhang J, Yang D, Thierry A, Wittmann JC, Lotz B (2001) Macromolecules 34:6261
16. Kawai T, Iijima R, Yamamoto Y, Kimura T (2002) Polymer 43:7301
17. Yan S, Katzenberg F, Petermann J, Yang D, Shen Y, Straupé C, Wittmann JC, Lotz B (2000) Polymer 41:2613
18. Garbarczyk J, Paukszta D (1981) Polymer 22:562
19. Park C, De Rosa C, Lotz B, Fetters LJ, Thomas EL (2003) Macromol Chem Phys 204:1514
20. Mathieu C, Thierry A, Wittmann JC, Lotz B (2000) J Polym Sci Part B Polym Phys 38:3088
21. Kopp S, Wittmann JC, Lotz B (1995) Macromol Symp 98:917
22. Fillon B, Lotz B, Thierry A, Wittmann JC (1993) J Polym Sci Part B Polym Phys 31:1395
23. Lovinger AJ, Davis DD, Lotz B (1991) Macromolecules 24:552
24. Asano T, Yan S, Petermann J, Yoshida S, Tohyama N, Imaizumi K, Sugiyama T (2003) J Macromol Sci Part B Phys 42:489
25. Yan S, Petermann J (2000) J Polym Sci Part B Polym Phys 38:80
26. Li H, Jiang S, Wang J, Wang D, Yan S (2003) Macromolecules 36:2802
27. Mathieu C, Thierry A, Wittmann JC, Lotz B (2000) Polymer 41:7241
28. Stocker W, Bickmann B, Magonov SN, Cantow HJ, Lotz B, Wittmann JC, Möller M (1992) Ultramicroscopy 42–44:1141
29. Wittmann JC, Lotz B (1990) Prog Polym Sci 15:909
30. Lotz B, Wittmann JC, Stocker W, Magonov SN, Cantow HJ (1991) Polym Bull 26:209
31. Thierry A, Mathieu C, Straupé C, Wittmann JC, Lotz B (2001) Macromol Symp 166:43
32. Stocker W, Magonov SN, Cantow HJ, Wittmann JC, Lotz B (1993) Macromolecules 26:5915
33. Haubruge HG, Daussin R, Jonas AM, Legras R, Wittmann JC, Lotz B (2003) Macromolecules 36:4452
34. Stocker W, Graff S, Lang J, Wittmann JC, Lotz B (1994) Macromolecules 27:6677
35. Grayer V, Lommerts BJ, Smith P, Lotz B, Wittmann JC (1995) Polymer 36:1915
36. Mathieu C, Stocker W, Thierry A, Wittmann JC, Lotz B (2001) Polymer 42:7033